

# BCS-like critical fluctuation with limited overlapping of Cooper pairs in FeSe

Huan Yang\*, Guanyu Chen, Xiyu Zhu, Jie Xing, and Hai-Hu Wen†

*National Laboratory of Solid State Microstructures and Department of Physics,  
Collaborative Innovation Center of Advanced Microstructures, Nanjing University, Nanjing 210093, China*

In conventional superconductors, very narrow superconducting fluctuation regions are observed above  $T_c$  because of the strong overlapping of Cooper pairs in a coherence volume  $4\pi\xi^3/3$  with  $\xi$  the coherence length. In the bulk form of iron chalcogenide superconductor FeSe, it is argued that the system may locate in the crossover region of BCS to BEC, indicating a strong superconducting fluctuation. In this respect, we have carried out measurements of magnetization, specific heat and Nernst effect on FeSe single crystals in order to investigate the superconducting fluctuation effect near  $T_c$ . The region of diamagnetization induced by superconducting fluctuation seems very narrow above  $T_c$ . The crossing point of temperature dependent magnetization curves measured at different magnetic fields, which appears in many systems of cuprate superconductors and is regarded as indication of strong critical fluctuation, is however absent. The magnetization data can be scaled based on the Ginzburg-Landau fluctuation theory for a quasi-two-dimensional system, but the scaling result cannot be described by the theoretical function of the fluctuation theory because of the limited fluctuation regions. The specific heat jump near  $T_c$  is rather sharp without the trace of strong superconducting fluctuation. This is also supported by the Nernst effect measurements which indicate a very limited region for vortex motion above  $T_c$ . Associated with very small value of Ginzburg number and further analyses, we conclude that the superconducting fluctuation is very weak above  $T_c$  in this material. Our results are strongly against the picture of significant phase fluctuation in FeSe single crystals, although the system has a very limited overlapping of Cooper pairs in the coherence volume. This dichotomy recalls a deeper insight on the superconducting mechanism when it is in the vicinity of Bose-Einstein condensation.

## I. INTRODUCTION

In iron pnictide/chalcogenide superconductors, a well accepted pairing symmetry is the spin-fluctuation mediated nodeless  $S\pm$  model, i.e., the superconducting gap changes its sign between the hole and electron pockets [1, 2]. In most cases, there are both structural and magnetic transitions in the doping dependent phase diagram. In addition, the antiferromagnetic (AFM) phase with an orthorhombic structure together with a nematic electronic state can even coexist with the superconducting phase in the underdoped region in many systems [3, 4]. Among the iron based superconductors, tetragonal FeSe has the simplest structure and its superconducting transition temperature  $T_c$  is about 9 K [5]. Surprisingly, only the structure transition from tetragonal to orthorhombic was observed at  $T_s \approx 90$  K in bulk FeSe without any trace of antiferromagnetic transition. Below  $T_s$  a significant electronic anisotropy is induced [6]. Fermi surfaces revealed by angle resolved photoemission (ARPES) and quantum oscillations [7–12] indicate the presence of hole and electron pockets with probably a strong non-degeneracy of the  $d_{xz}$  and  $d_{yz}$  orbitals. This leads to the breaking of the fourfold symmetry in the orthorhombic phase below  $T_s$ . Regarding the very shallowed band top or bottom, it was argued that the Fermi energy is quite small and the effective charge carrier density in the material is very dilute. On the other hand, the superconducting transition temperature of FeSe can be easily enhanced to about 38 K at a pressure of 6 GPa, and there is also a pressure-induced magnetic transition dome in a wide pressure range [13, 14]. The stripe-type spin

fluctuations are also observed below  $T_s$  and almost independent of pressure, which reconciles FeSe with other iron-based superconductors [15]. Furthermore, another interesting issue for superconductivity in FeSe is about the exact structure of superconducting gap, which is still under debate. The V-shaped tunneling spectra observed by earlier scanning tunneling spectroscopy (STS) measurements on FeSe film [6] was argued as the evidence of d-wave superconducting gap. This was corroborated by STM measurements on FeSe single crystals, and the tiny fully gapped states near the Fermi level was ascribed to the effect of the twin boundaries [16]. However, the nodeless gap feature is suggested by the thermal conductivity [17] and specific heat measurements [18, 19]. Recently, a pair of nodeless sign-reversal gaps with extremely high anisotropy are detected with very detailed Bogoliubov quasiparticle interference analysis based on the STS measurements [20].

In a conventional superconductor, the superconducting pairing and condensation both occur at  $T_c$ , and the superconducting fluctuation (SCF) region is very limited above  $T_c$ . This is because there are great number of Cooper pairs in the coherence volume  $4\pi\xi^3/3$  with  $\xi$  the coherence length. In other words, the Cooper pairs are strongly overlapped each other in space. Actually the Cooper pairs in the coherence volume  $4\pi\xi^3/3$  in conventional superconductors can be understood as the highly entangled state of thousands of Cooper pairs. In high- $T_c$  cuprate superconductors, however, the SCF has been shown to be quite strong. This strong SCF was interpreted as the existence of strong phase fluctuation of preformed Cooper pairs above  $T_c$ . This picture has been

proved by the observation of very large Nernst signal and diamagnetic magnetization far above  $T_c$  [21]. However, the temperature range of SCF in iron-based superconductors seems not so wide [22–27] except in  $\text{CsFe}_2\text{As}_2$  [28]. Recently, it is suggested that the SCF may be very strong in FeSe single crystals because of the vicinity to the Bose-Einstein condensate (BEC) and Bardeen-Cooper-Schrieffer (BCS) crossover region of the material [29, 30]. This recommends a picture of preformed Cooper pairs with phase incoherence far above  $T_c$  in FeSe.

In this work, we carry out careful measurements with multiple tools on FeSe single crystals, in order to get further information about the SCF effect above  $T_c$ . We observe BCS mean-field like SCF in a rather narrow temperature region in this material, which is similar to the situation in other iron based superconductors, such as optimally doped  $\text{Ba}_{1-x}\text{K}_x\text{Fe}_2\text{As}_2$ . This may be attributed to the very small Ginzburg number in all of these systems. However, when counting the conduction electrons in the coherence volume, we indeed find that the density of the Cooper pairs in real space is very diluted, near the crossover region of BEC to BCS.

## II. EXPERIMENTAL TECHNIQUES

High-quality FeSe single crystals are grown by chemical vapor transport method with the eutectic mix of KCl and  $\text{AlCl}_3$  as the transport agent [31].  $\text{Fe}_{1.04}\text{Se}$  polycrystals were grown as the starting materials by solid state reaction. The mixture of  $\text{Fe}_{1.04}\text{Se}$ , KCl and  $\text{AlCl}_3$  (molar ratio 1:2:4) was put into the bottom of a quartz ampoule, and the quartz ampoule was sealed under vacuum. The quartz ampoule was then placed into a horizontal tube furnace and heated up to 430 °C. After keeping temperature for 30 hours to melt the transport agent, the temperature of one end of the ampoule without reactant was lowered down to 370 °C to make a temperature gradient. We kept sintering the sample with this temperature gradient for 6 weeks and FeSe single crystals with tetragonal structure were synthesized at the colder end of the ampoule.

The resistivity was measured with a Quantum Design Physical Property Measurement System (PPMS) by conventional four-probe method at different fields. The magnetization results were measured by a Quantum Design instrument SQUID-VSM with magnetic field up to 7 T, and the magnetic field was applied parallel to the  $c$ -axis of the sample in the measurements. The specific heat was measured with thermal-relaxation method as an option of the Quantum Design PPMS. The Nernst effect was measured by the one-heater-two-thermometer technique on a home-made setup attached to PPMS. A temperature gradient along the length direction is established by a heater and the temperature difference is measured by a pair of type-E thermocouples in the measurements of Nernst signal. The transverse voltage of the Nernst signal is measured at a magnetic field perpendicular to the

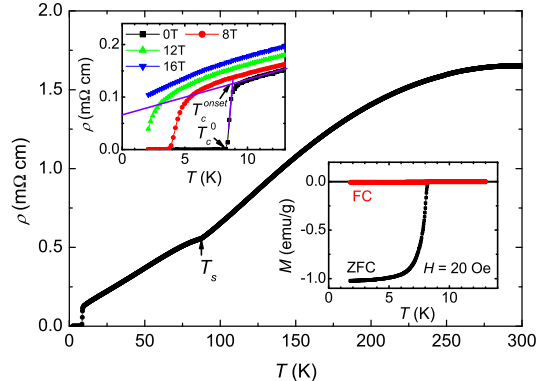


FIG. 1. (Color online) Temperature dependence of resistivity at zero magnetic field. The upper left inset shows the resistivity measured at magnetic fields of 0, 8, 12 and 16 T, and the bottom right inset shows the temperature dependence of magnetization measured in zero-field-cooled (ZFC) and field-cooled (FC) modes at 20 Oe.

thermal current in the  $ab$ -plane, and the data are taken with both positive and negative fields to reduce the interference of thermopower signal which is field symmetric.

## III. RESULTS

### A. Magnetization and analysis near $T_c$

Temperature dependence of zero-field-cooled (ZFC) and field-cooled (FC) magnetization measured at 20 Oe are shown in the bottom right inset of Fig. 1. The bulk superconducting transition temperature determined from the onset of magnetization transition is about 8.7 K from the enlarged view near  $T_c$ , and the superconducting volume calculated from the magnetization data is about 138% when the demagnetization factor is roughly calculated. The value beyond 100% is induced by the difficulty in precisely determining the demagnetization factor for a sample with a rectangular bar shape. The temperature dependence of resistivity  $\rho(T)$  at zero magnetic field is shown in Fig. 1. We can see a clear kink at  $T_s \approx 87.4$  K which is caused by the structural transition from tetragonal to orthorhombic phase, or the establishment of the nematic state. The superconducting transition temperature  $T_c^{\text{onset}}$  determined in the upper left inset of Fig. 1 using the usual crossing method is about 8.8 K, and zero resistivity occurs at  $T_c^0 = 8.3$  K with transition width of about 0.5 K. The residual resistivity ratio  $RRR = \rho(300 \text{ K})/\rho(0 \text{ K})$  is about 25. The zero temperature resistivity  $\rho(0 \text{ K})$  is determined through a linear fit of the low temperature data between 10 to 15 K. The resistivity curves measured at magnetic fields shows a clear enhancement compared to that measured

at zero field, and the magnetoresistance ( $MR$ ) calculated by  $MR = [\rho(16 \text{ T}) - \rho(0 \text{ T})] / \rho(0 \text{ T})$  is about 43% at 10 K. This  $MR$  value is much smaller than the ones from previous reports [29, 30]. However it should be noted that the huge magnetoresistance in previous report [29, 30] is followed by an insulating-like upturn in low temperature region. This giant  $MR$  in those work suggests that some exotic physics may be involved here, for example it is more or less similar to the pressure induced resistance upturn associated with some magnetic ordering [13, 14], or due to the quantum oscillation effect and the density of states (DOS) shows a significant decreasing under the magnetic field. The excess conductivity defined as  $1/[\rho_n(T) - \rho(T)]$  with  $\rho_n$  the linear extrapolation of the normal state resistivity, may be caused by the existence of residual Cooper pairs above bulk  $T_c$ . Strong excess conductivity is usually regarded as the mark of SCF. We note that, as shown in the up left inset of Fig. 1, the excess conductivity shows a very gentle variation in high temperature region, it is very difficult to define the end point of excess conductivity and the SCF region. Thus we measure magnetization in the temperature region near  $T_c$  to check how strong the SCF is in the material.

To detect SCF in FeSe, we measure the magnetization at different magnetic fields, and temperature dependent magnetization  $M$  curves measured with zero-field-cooled (ZFC) and field-cooled (FC) mode at fields of 0.5, 1, 2, 3, 4, 5, 6 and 7 T are shown in Fig. 2(a). There is a large positive magnetization background for each field in the normal state, which may make the weak diamagnetization arising from the SCF invisible. In order to get the net contribution induced by the possible SCF, we fit the ZFC magnetization data in the normal state by the Curie-Weiss law. The positive magnetization background in the normal state is originated from paramagnetic impurities and Pauli paramagnetism of the conduction electrons, which is supported by the monotonically increase of  $M$  with decrease of temperature above  $T_c$ . We then fit the ZFC magnetization data in the normal state by Curie-Weiss law as,

$$M = M_0 + C_0/(T + T_\theta) \quad (1)$$

with  $M_0$ ,  $C_0$  and  $T_\theta$  the fitting parameters. The first term  $M_0$  in Eq. 1 represents mainly the Pauli paramagnetization part contributed by conduction electrons. The second term,  $C_0/(T + T_\theta)$  is contributed by the magnetic moments in the sample, where  $T_\theta$  denotes the Weiss temperature. The fitting parameters at various fields are shown in Table. I.

The fitting curves are shown by solid lines in Fig. 2(a). One can see that the Curie-Weiss law works very well to describe the experimental data in the normal state. The deviation point between the magnetization curve and the fitting curve is defined as onset temperature  $T_{c,M}^{onset}$  at which the upper critical field  $\mu_0 H_{c2}$  equals to the applied magnetic field. A particular case for 7 T is shown as an enlarged view in Fig. 2(b). Although there is an uncertainty in defining the very onset temperature  $T_{c,M}^{onset}$ , one

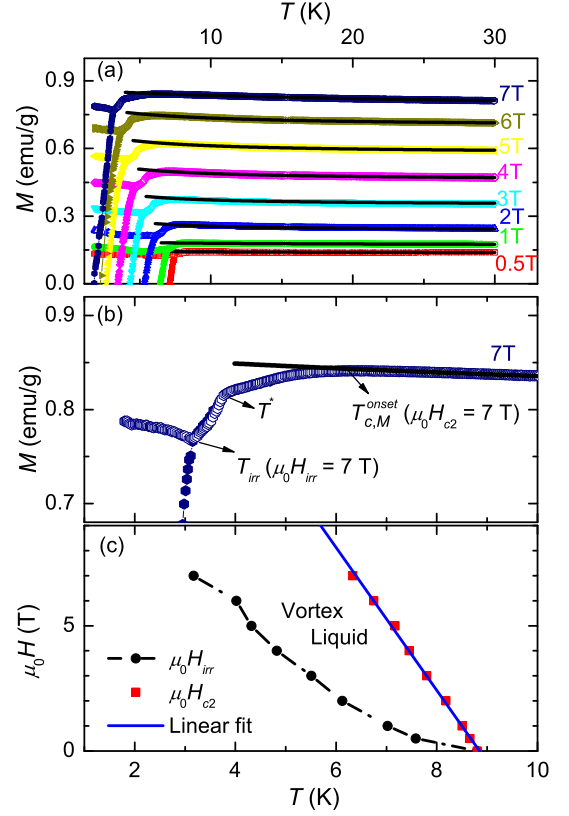


FIG. 2. (Color online) (a) Temperature dependence of mass magnetization measured at different magnetic fields. The solid and open symbols are the data measured with zero-field-cooled and field-cooled mode, respectively. The black solid lines are the fitting curves by using Curie-Weiss law. (b) The enlarged view of the magnetization data at 7 T and the definitions of characteristic temperatures at characteristic magnetic fields. (c) The  $\mu_0 H$ - $T$  vortex phase diagram of FeSe from the magnetization measurements. The filled squares represent the experimental data of  $\mu_0 H_{c2}(T)$ . The solid blue line is a linear fit to the upper critical field  $\mu_0 H_{c2}(T)$  near  $T_c$ .

can see that the allowed region of temperature is quite narrow, of about  $\pm 1$  K. We can also determine the irreversible temperature  $T_{irr}$  by taking the separation point of ZFC and FC magnetization curves, and at that temperature  $\mu_0 H_{irr} = 7$  T in Fig. 2(b). It should be noted that there is a kink in the magnetization curves between  $T_{c,M}^{onset}$  and  $T_{irr}$ , which is marked as  $T^*$  and is also field dependent. The characteristic temperature  $T^*$  may be caused by some unknown vortex phase transition in the vortex liquid region, and it needs further experimental investigation. We leave the discussion on  $T^*$  to a separate study. The  $\mu_0 H$ - $T$  phase diagram of FeSe shown in Fig. 2(c) displays the temperature dependent behaviors of  $\mu_0 H_{c2}$  and  $\mu_0 H_{irr}$ . One can find that the vortex liquid region in the phase diagram is not so wide. And the almost linear temperature dependent  $\mu_0 H_{c2}$  near  $T_c$  gives rise to a slope  $d\mu_0 H_{c2}/dT = -2.85$  T/K near  $T_c$ ,

TABLE I. The parameters derived from fitting to the  $M$ - $T$  data in Fig. 2(a) by using Curie-Weiss law as Eq. 1.

$\mu_0 H$ (T)	$M_0$ (emu/g)	$C_0$ (emu-K/g)	$T_\theta$ (K)
0.5	0.13	0.11	17.17
1	0.17	0.15	8.34
2	0.23	0.19	0.10
3	0.35	0.25	1.21
4	0.46	0.35	2.48
5	0.58	0.45	3.47
6	0.70	0.55	4.91
7	0.77	2.20	24.67

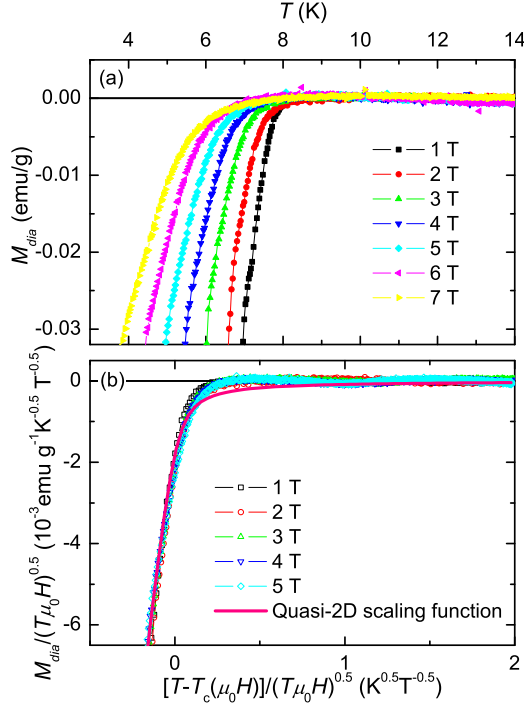


FIG. 3. (Color online) (a) Temperature dependence of diamagnetic magnetization  $M_{dia}$  at different field obtained by subtracting the fitted background by Eq. 1 from the experimental data. (b) Scaling curves from (a) by using the Ginzburg-Landau fluctuation theory for a quasi-2D system. The solid line is the expected scaling function of the quasi-2D scaling theory.

and the calculated  $\mu_0 H_{c2}(0)$  at zero temperature by the Werthamer-Helfand-Hohenberg (WHH) formula [32], i.e.,  $\mu_0 H_{c2}(0) = 0.69 T_c |d\mu_0 H_{c2}/dT|_{T_c}$  is about 15.7 T. This is consistent with previous report [29]. We emphasize that, from our data and analysis, the SCF region is quite limited. For example, at a field of 7 T, the upper limit temperature for SCF is about 7 K.

In order to investigate the SCF in FeSe, Ginzburg-Landau fluctuation theory is used to analyze the diamagnetic signal near  $T_c$ . Since the normal state has a background of magnetization, we need to subtract this

part from the total signal. The magnetization arising from superconductivity (including SCF) ( $M_{dia}$ ) shown in Fig. 3(a) are obtained by subtracting the fitted paramagnetic background (Curie-Weiss term) from the measured magnetization. One can see that  $M_{dia}$  approaches to zero just above  $T_c$ , which indicates that the SCF is very weak. Usually a common crossing point or a small crossing area appears on the set of  $M$ - $T$  curves at different magnetic fields in a superconductor with strong SCF, which can be well described by quasi-two-dimensional (quasi-2D) or three-dimensional (3D) lowest Landau level (LLL) scaling formula based on Ginzburg-Landau (GL) theory [33]. This has been well checked in cuprate superconductors [34, 35]. However, we find that the  $M_{dia}(T)$  curves in our present sample separate from each other and show no crossing point or area expected by the GL-LLL scaling theory. Although this situation suggests that the scaling theory does not work in this system, we still try to scale the  $M_{dia}$ - $T$  curves by following the scaling law to obtain further comprehension. By using a non-perturbative approach to the GL free energy function for a quasi-2D system, the  $M(T)$  curves can be scaled by

$$M/(T\mu_0 H)^{0.5} = Cf \left\{ \frac{A[T - T_c(\mu_0 H)]}{\sqrt{T\mu_0 H}} \right\}, \quad (2)$$

where

$$f(x) = x - \sqrt{x^2 + 2}, \quad (3)$$

and the field dependent  $T_c$  is expressed as

$$T_c(\mu_0 H) = T_{c0} - \mu_0 H \left( \frac{d\mu_0 H_{c2}}{dT} \right)^{-1}. \quad (4)$$

Here  $T_{c0}$ ,  $d\mu_0 H_{c2}/dT$ ,  $A$ , and  $C$  in Eq. 2,4 are the scaling parameters. The parameter  $A$  is dependent on the GL parameter  $\kappa$  and  $|d\mu_0 H_{c2}/dT|_{T_c}$ , and  $C$  is inversely proportional to  $\kappa$ , in addition both of  $A$  and  $C$  are independent of  $H$  or  $T$ . The quasi-2D scaling curves at different fields in FeSe are shown in Fig. 3(b), where  $M_{dia}/(T\mu_0 H)^{0.5}$  is scaled as a function of  $[T - T_c(\mu_0 H)]/(T\mu_0 H)^{0.5}$ . Surprisingly, the quasi-2D fluctuation scaling law works well on the data measured from 1 T to 5 T although there is no crossing point for the  $M_{dia}$ - $T$  curves. The data at 6 and 7 T show clear deviation from the scaling and are not shown here. The parameters  $T_{c0}$  and  $d\mu_0 H_{c2}/dT$  obtained from the scaling process are 8.12 K and  $-2.13$  T/K respectively, which are close to the values obtained in the resistive and magnetization measurements. We have also tried the 3D GL fluctuation scaling, which does not work on the data. The absence of crossing point in  $M_{dia}$ - $T$  curves and the nice quasi-2D fluctuation scaling behavior seem contradictory in this material. However, as shown by the solid line in Fig. 3(b), the scaled curves have clear deviations from the scaling function of Eq. 3. The difference between the scaling curves and the required scaling function is more pronounced in the fluctuation region, and

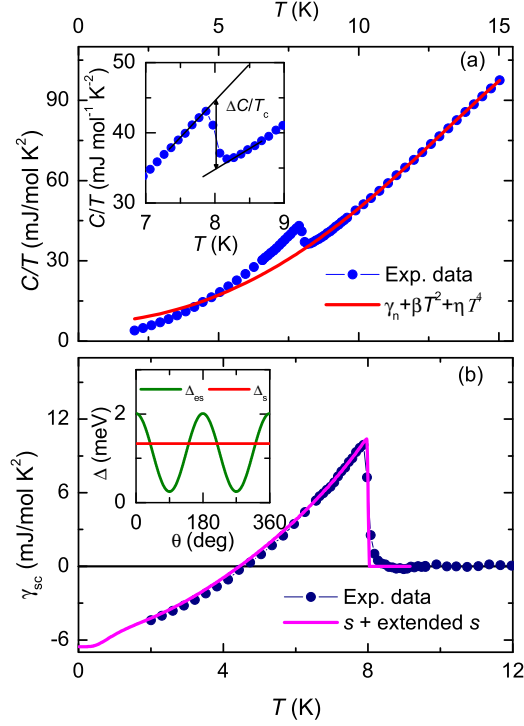


FIG. 4. (Color online) (a) Temperature dependent specific heat measured at 0 T. The red solid line is the normal state fitting curve. The inset shows the enlarged view of the specific heat jump near  $T_c$ , and  $\Delta C/T_c$  is estimated by entropy conservation near  $T_c$ . (b) Temperature dependence of superconducting electronic specific heat. The transition temperature  $T_c^{SH}$  from specific heat jump estimated by entropy conservation as show in (b) or the inset in (a) is about 8 K. The blue line represents the fitting curve by using the BCS formula. The inset shows the angle dependent gap functions used in the fitting.

the scaled curves show much narrower SCF region compared with the quasi-2D scaling function shown by the pink solid line here. Therefore, the scaling behavior in FeSe can not be described by the GL-LLL scaling theory, which is consistent with the absence of the crossing point in the diamagnetic magnetization curves.

### B. BCS mean-field like transition detected by specific heat measurement

The specific heat measurement is a useful tool to detect the SCF near  $T_c$ . The temperature dependence of specific heat at 0 T is presented in Fig. 4(a). As we can see from the enlarged view in the inset of Fig. 4(a), there is a sharp jump  $\Delta C/T_c$  near the superconducting transition. The specific heat jump estimated by entropy conservation yields the ratio  $\Delta C/\gamma_n T_c = 1.46$ , which is close to 1.43 predicted by BCS theory in the weak coupling regime.

In order to obtain the superconducting electronic specific heat, we fit the data of normal state above  $T_c$  by  $C_n/T = \gamma_n + \beta T^2 + \eta T^4$ , where  $\gamma_n$  is the normal state electronic part, and  $\beta T^2 + \eta T^4$  is the phonon contribution by Debye model in low temperature region. The fitting result is shown by the red solid line in Fig. 4(a), and the parameters obtained by the fitting process are  $\gamma_n = 6.7 \text{ mJ}\cdot\text{mol}^{-1}\cdot\text{K}^{-2}$ ,  $\beta = 0.41 \text{ mJ}\cdot\text{mol}^{-1}\cdot\text{K}^{-4}$  and  $\eta = 3.4 \times 10^{-4} \text{ mJ}\cdot\text{mol}^{-1}\cdot\text{K}^{-6}$ . Temperature dependence of superconducting electronic specific heat obtained by the equation  $\gamma_{sc} = C_{sc}/T = (C - C_n)/T$  is shown in Fig. 4(b), and then we fitted the data by BCS formula. The superconducting electronic specific heat  $\gamma_{sc}$  for an anisotropic superconducting gap can be expressed as

$$\gamma_{sc} = \frac{4N(E_F)}{k_B T^3} \int_0^{+\infty} \int_0^{2\pi} \frac{e^{\zeta/k_B T}}{(1 + e^{\zeta/k_B T})^2} \cdot \left[ \varepsilon^2 + \Delta^2(\theta, T) - \frac{T}{2} \frac{d\Delta^2(\theta, T)}{dT} \right] d\theta d\varepsilon, \quad (5)$$

where  $\zeta = \sqrt{\varepsilon^2 + \Delta^2(T, \theta)}$ . A linear combination of two components with different gaps, namely,  $\gamma_{sc} = x\gamma_{sc1}(\Delta_s) + (1-x)\gamma_{sc2}(\Delta_{es})$ , is used to describe the experimental data as previous report [36]. The gap functions we used are an  $s$ -wave  $\Delta_s$  and an extended nodeless  $s$ -wave  $\Delta_{es} = \Delta_{es}^0(1 + \alpha \cos 2\theta)$ . A set of fitting parameters we choose for the experimental data are  $\Delta_s(0) = 1.33 \text{ meV}$ ,  $\Delta_{es}^0(0) = 1.13 \text{ meV}$ ,  $x = 0.2$ , and  $\alpha = 0.78$ . The angle dependent gap functions used for the fitting are shown in the inset of Fig. 4(b), and the fitting curve is shown as the solid curve in Fig. 4(b) with a very sharp transition at  $T_c^{SH} = 8 \text{ K}$ . We should notice that it is difficult to obtain the precise gap structure by fitting using the data in Fig. 4(a) because of the lack of data measured at extremely low temperatures. This will be presented in a separate publication [19]. Here we want to emphasize that the specific heat anomaly near  $T_c$  is very sharp and it is BCS mean field like. A modified gap function [36] will have very little influence on the shape of specific heat jump near  $T_c$ . One can clearly see that, the temperature range of SCF illustrated by the extending tail of  $\gamma_{sc}$  above  $T_c^{SH}$  is very narrow, and the highest fluctuation temperature can only be extended to about 9 K. This value is quite close to the onset transition temperatures from the transport and magnetization measurements. Therefore, the specific heat data near the superconducting transition can be well described by BCS mean field approach, which confirms the narrow fluctuation region in FeSe.

In the framework of BCS-Eliashberg mean-field theory, the formation and condensation of Cooper pairs will take place at the same temperature  $T_c$  [37]. However, if phase fluctuation is too strong, the Cooper pairs may preform at some temperature  $T^*$  higher than the Cooper-pair condensation temperature  $T_c$ , hence there will be a wide temperature range of residual superconductivity between  $T_c$  and  $T^*$  [38]. The difference between the two theories mentioned above can be easily distinguished by the shape of the specific heat curve near  $T_c$  [39]. In the



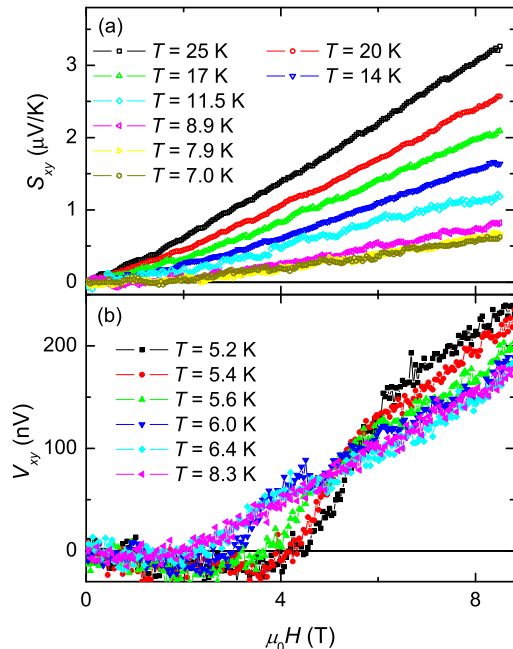


FIG. 5. (Color online) (a) Field dependent Nernst signal  $S_{xy}$  at different temperatures above 7 K. (b) Field dependence of Nernst transverse voltage  $V_{xy}$  at different temperatures with tiny exchange helium gas to lower down the base temperature of the sample.

ideal BCS mean field case, a second-order phase transition takes place at  $T_c$ , which leads to a very sharp jump in specific heat. In the system with moderate SCF, a  $\lambda$ -shaped transition of specific heat coefficient will be observed, i.e., the high-temperature end point  $T^*$  is a bit away from  $T_c$ . If the SCF is strong enough, temperature difference between the real-space pairing and the bulk superconductivity governed by BEC is very large, and the specific heat decreases smoothly from  $T_c$  to  $T^*$  which is similar as the situation in the  $\lambda$ -transition of  $^4\text{He}$  [39]. As we can see from the data in FeSe, the specific heat data shows only a very small tail above  $T_c^{SH}$ , which can be described rather well by the BCS mean field transition and is very different from the picture of BEC.

### C. Narrow SCF region verified by Nernst effect

The vortices in the flux-flow state of a superconductor carry entropy within and nearby the vortex core, and they will move from the hot end to the cold one of the sample with temperature gradient. Transverse Nernst signal is sensitive to the vortex motion when the magnetic field is applied perpendicular to the thermal current. The field (or temperature) dependent Nernst signal  $S_{xy} = E_y/\partial_x T$  at some fixed temperature (or field) dom-

inated by vortex motion is usually hump-like. It means that  $S_{xy}$  starts from zero when the vortices start moving, and reaches its maximum at some magnetic field (or temperature), then decreases with increasing of magnetic field (or temperature) and disappears in the normal state. Thus the Nernst signal in the flux flow region and at a fixed temperature can be written as  $S_{xy} \propto H(1 - H/H_{c2})$  [40]. The Nernst signal can have a small tail above bulk  $T_c$  or  $H_{c2}$  because of the SCF [41]. However, in cuprates, it was found that the Nernst signal has a hump-like field dependence in a very wide temperature range above  $T_c$ , which is regarded as the strong SCF [21].

So we measure the Nernst effect to detect the SCF in FeSe. The field dependent curves of Nernst signal  $S_{xy}$  at different temperature above 7 K are presented in Fig. 5(a). One can find that  $S_{xy}$  is almost proportional to the magnetic field and with a very weak contribution from quadratic or higher-order field term. In a single-band metal, the Nernst coefficient  $\nu_{xy} = S_{xy}/\mu_0 H$  is very small because of the cancellation effect between the thermal and the coulomb contributions [41]. However, the value of  $\nu_{xy}$  in FeSe seems very large even if compared with the typical multiband material NbSe<sub>2</sub> [42]. The almost linear field dependent Nernst signal with a slight positive curvature above  $T_c$  is obviously from the normal-state properties, such as the bi-parity motion of electron and hole-like charge carriers. Even when the temperature decreases just below  $T_c$ , there is no obvious hump feature or negative second derivative originated from the vortex motion. The Nernst signal measurements are usually carried out at high vacuum to measure the exact value of the temperature gradient, however the lowest temperature of the sample with heating power is only about 6.5 K in our home-made measurement system in PPMS. So we add some exchange helium gas to the measurement chamber to lower down the temperature when measuring the Nernst signal at low temperatures. In this case, we cannot measure the exact temperature gradient, but the same heating power is used at temperature up to 8.3 K with an overlapped temperature range as the exact  $S_{xy}$  measurements. Since the temperature range is about 3 K in the measurements, we can regard the temperature gradient as a constant in these measurements. We plot the Nernst voltage  $V_{xy}$  in Fig. 5(b), and the relatively large voltage noise is caused by the temperature fluctuation from the exchange gas.

The temperature dependent Nernst coefficient  $\nu_{xy}$  and amplified  $V_{xy}$  measured with exchange gas are shown in Fig. 6. One can see that the Nernst coefficient has a huge hump with maximum value as large as  $0.9 \mu\text{V}\cdot\text{K}^{-1}\cdot\text{T}^{-1}$  below and near the structural transition temperature  $T_s$ . Similar data have been measured on the parent compounds of iron pnictides with both structural transition and spin-density-wave (SDW) transition [43–45]. Such a large Nernst signal with a hump like temperature dependence are quite often observed below the SDW transition temperature, so it is suggested that the SDW order or SDW fluctuation may enhance the Nernst coefficient

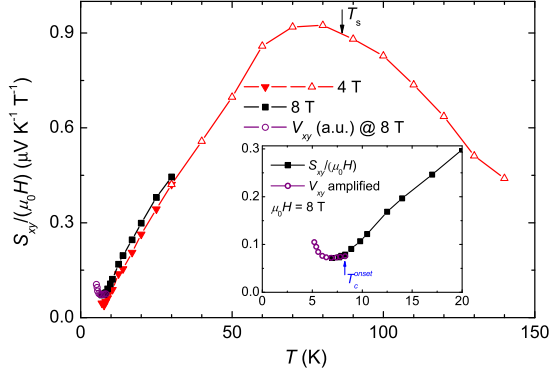


FIG. 6. (Color online) Temperature dependence of the Nernst coefficient at different fields. The filled symbols represent the data obtained by the field dependent Nernst signal. The hollow triangles are Nernst coefficients measured at 4 T and different temperatures. Nernst voltage values measured with some exchange helium gas are shown as the hollow circles with the arbitrary unit, i.e., the  $V_{xy}$  values are multiplied by a necessary factor to make the data have a smooth connection to the Nernst signal  $S_{xy}$  measured at the same field and temperature. The inset shows the enlarged view of Nernst coefficient at low temperatures and 8 T.

[27]. However, there is only structural transition in FeSe without any magnetic order in the sample at zero pressure [15]. One of the explanations for the huge Nernst coefficient is some possible spin fluctuation in FeSe which is too weak to be observed on the sample. It should be noted that the Hall coefficient in all these material with huge Nernst peaks seems very small and even has a sign change with increasing temperature. So another possibility of the huge Nernst signal may come from the almost balanced hole and electron pockets [42], and the the drastic change of the Nernst signal near  $T_s$  may be induced by the change of Fermi surface near the structural transition.

In the temperature region below  $T_c$ , the Nernst coefficient shows a small enhancement with decreasing temperature. At the lowest temperature we measured, for example  $T = 5.2$  K here, the Nernst signal is zero below 4 T, then it ramps up at higher fields, as shown in Fig. 4(b). At a field of about 6 to 7 T, the curve shows a negative curvature and merges into the background of the normal state. Similar situation occurs for the data at temperatures up to 6.4 K, although the threshold of magnetic field for flux flow now becomes much smaller. This phenomenon is regarded as the typical feature of vortex flow on top of a large signal of background, although we did not obtain the peak of Nernst signal in whole region. The absence of a peak due to flux flow is because the Nernst signal due to vortex motion is very small comparing with that of the normal state background. Therefore, one can see that the Nernst coefficient shown in Fig. 6 from the vortices become negligible near and above  $T_c$ ,

which is consistent with the conclusion from field dependent Nernst signal. The Nernst effect measured in FeSe is similar to the situation in  $\text{Fe}_{1+y}\text{Te}_{0.6}\text{Se}_{0.4}$  in which the SCF is very weak and the amplitude of the peak of Nernst signal from the vortices is also very small [24]. In electron doped cuprates, one also see very similar situation, the Nernst signal with a very small peak structure appears on top of a large background due to bi-parity contributions [46]. One explanation for this very small Nernst signal is that the vortices in FeSe or Te doped FeSe may carry very little entropy, together with the fact that the vortex liquid region is very small. In any case, we can conclude that no vortex motion induced Nernst signal is observed above  $T_c$ .

#### D. Revisit the calculation of the Ginzburg number

The SCF in a superconductor can be treated approximately by the GL theory, and the magnitude of SCF can be characterized by the Ginzburg number [47]

$$Gi = (k_B T_c / \mu_0 H_c^2 \epsilon \xi^3)^2 / 2. \quad (6)$$

Here the thermodynamic critical field  $\mu_0 H_c = \mu_0 H_{c2} / (\sqrt{2}\kappa)$ , and the upper critical field  $\mu_0 H_{c2}$  is obtained by extrapolating the linear part of  $\mu_0 H_{c2}(T)$  near  $T_c$  and calculated [48] by using the WHH formula  $\mu_0 H_{c2}(0) = -0.69 T_c [d\mu_0 H_{c2}(T)/dT]_{T_c}$ , instead of using the measured value of  $\mu_0 H_{c2}(0)$ . The anisotropy parameter  $\epsilon \equiv \sqrt{m_{ab}^*/m_c^*} = H_{c2}^c / H_{c2}^{ab}$  is usually smaller than 1. Considering the relationship between  $H_{c2}$  and coherence length  $\xi$ , i.e.,  $\xi = \sqrt{\phi_0 / 2\pi\mu_0 H_{c2}}$ , the Ginzburg number  $Gi$  calculated in the SI unit reads

$$Gi = 1.7 \times 10^{-11} T_c^2 \kappa^4 / (\mu_0 H_{c2} \epsilon^2). \quad (7)$$

Here the coefficient and all the parameters are in SI units. It should be noted that the original calculation in Ref. 48 have some mistakes in using the value of  $\mu_0$  in cgs units, therefore the exact value of the frequently discussed  $Gi$  should be multiplied by a factor of  $(4\pi)^2$ . Because of this error, in high- $T_c$  cuprate superconductors, the mistakenly used Ginzburg number is supposed to be  $Gi \approx 10^{-3} \sim 10^{-1}$ , while the value is extremely small ( $Gi \approx 10^{-8} \sim 10^{-6}$ ) in conventional superconductors [47]. However, as just mentioned, the real values of  $Gi$  should be multiplied by  $(4\pi)^2$ , which enhances  $Gi$  two orders of magnitude larger than the previously widely used ones. We want to emphasize that, in order to have a meaningful discussion on the SCF and its region,  $Gi$  should be much smaller than 1, but the calculated value of  $Gi$  in some cuprates, like Bi2212, may be greater than 1. Although such large value of  $Gi$  is not meaningful, it may just suggest the strong fluctuation in the sample. In addition, the temperature range of SCF is determined simply by the Ginzburg number as  $Gi T_c$  where  $Gi$  seems to be too small in the original calculation [48]. For example, for  $\text{YBa}_2\text{Cu}_3\text{O}_{7-\delta}$  (YBCO), the calculated  $Gi$  using

TABLE II. Characteristic superconducting parameters of different superconductors.

	Bi2212	YBCO	MgB <sub>2</sub>	BaK122	FeSe
$T_c$ (K)	95	91	39	38	8.2
$\mu_0 H_{c2}$ (T)	177	180	4	180	16
$\kappa$	115	62	21	80	72
$\epsilon$	0.02	0.24	0.5	0.5	0.55
$Gi$	380	$2 \times 10^{-1}$	$5 \times 10^{-3}$	$2.2 \times 10^{-2}$	$6.4 \times 10^{-3}$
$T_c/T_F$	0.035	0.011	0.007	0.17	0.2
$k_F \xi$	-	-	23	4	3
$V_{coh} n_{pair}$	1	109	$1.5 \times 10^5$	122	31

original formula is 0.00127, and the SCF region will be only 0.11 K. This is unreasonable. Therefore a factor of  $(4\pi)^2$  should be multiplied to the original formula, or the correct form of calculating the  $Gi$  is Eq. 7.

In the following, we have a rough estimation on the values of  $Gi$  and the SCF regions for different superconductors. The typical superconducting parameters and calculated  $Gi$  for Bi<sub>2</sub>Sr<sub>2</sub>CaCu<sub>2</sub>O<sub>8</sub> (Bi2212) [49–51], YBCO [50–54], MgB<sub>2</sub> [50, 51, 55, 56], Ba<sub>0.6</sub>K<sub>0.4</sub>Fe<sub>2</sub>As<sub>2</sub> (BaK122) [51, 57–60], and FeSe [29, 61, 62] are presented in Table II. Here  $\mu_0 H_{c2}$  is determined from the value of  $d\mu_0 H_{c2}/dT$  near  $T_c$ . The calculated  $Gi$  for BaK122 or FeSe are much smaller than those in Bi2212 or YBCO, but comparable with the value in MgB<sub>2</sub>. Meanwhile it is claimed that another calculation method for  $Gi$  in a 2D system is to determine the ratio  $T_c/T_F$ , and it is of the order of  $10^{-1}$  in BEC limit and  $10^{-5} \sim 10^{-4}$  for BCS superconductors [63]. The calculated values of  $T_c/T_F$  from  $E_F$  in 2D cuprate superconductors Bi2212 and YBCO presented in Table II are very small because of the large Fermi energy, and the value of FeSe is comparable with the one in BaK122. This seems to contradict with the situation that Bi2212 is a typical superconductor with very strong SCF, and people even argue that the superconductivity in Bi2212 is governed by a BEC-like transition [39]. Actually the strong SCF in Bi2212 is more driven by the strong anisotropy (or small  $\epsilon$ ). Therefore the ratio  $T_c/T_F$  may not be a good parameter to determine the fluctuation behavior of a superconductor. In addition, for a 3D system, the  $Gi$  is determined [63] by  $80(T_c/T_F)^4$ , the value of  $Gi$  is further lowered down. For iron based superconductors, such as FeSe and BaK122, it is more close to the case of 3D, thus a simple estimation of  $Gi \approx T_c/T_F$  may give problem. Furthermore, for a system with multi-bands, if some bands have large Fermi energies, but others have very small values, the superfluid coming from the band with large Fermi energy may stabilize the condensation and suppress the SCF. Thus, a correct way to estimate SCF is to use Eq. 7. These arguments may provide answers to our observation that the SCF in bulk FeSe is not strong.

#### IV. DISCUSSION AND COUNTING ON THE OVERLAPPED COOPER PAIRS

In the BCS theoretical picture, the Cooper pairing and condensation occur simultaneously. In this framework, it is meaningless to describe a Cooper pair in real space. One can only say that many electrons form a highly entangled paired state. The basic reason for that is the strong overlapping between Cooper pairs. Therefore in this model, tens of thousands of Cooper pairs are overlapping each other. The product of the Fermi vector  $k_F$  and coherence length  $\xi$ , is a very good quantity to estimate how strong the overlapping is. The quantity  $k_F \xi$  tells roughly how much conduction electrons or Cooper pairs in one coherence length. Thus this parameter is also used to define the crossover from BCS to BEC [64] when  $k_F \xi \approx 1$ . And  $k_F \xi \geq 2\pi$  is corresponding to BCS-like superconductivity, while  $k_F \xi \leq 1/\pi$  is corresponding to the BEC case. Taking the related quantities from experiment, we find that both FeSe and BaK122 have the value  $k_F \xi$  smaller than  $2\pi$ , so they may be near the crossover region from BCS to BEC but much closer to BCS according to the calculation of the chemical potential [64]. To consider the situation in 3D case, the number of superconducting electrons in unit coherent volume  $V_{coh} n_{pair}$  can also be used [65] to determine the different situations between BCS and BEC, and  $n_{pair} = n_s/2$  is the density of the superconducting electrons with opposite momentum which can be paired with the selected electron while coherent volume  $V_{coh} = 4\pi \xi_{ab}^2 \xi_c/3$  for an anisotropic superconductor. Following above discussions, we expect  $V_{coh} n_{pair} \gg 1$  in the BCS case, while  $V_{coh} n_{pair} \ll 1$  for the BEC limit [66]. The evolution from BCS to BEC transition is accompanied with the significant reduction of  $V_{coh} n_{pair}$ . We replace  $n_s$  with charge carrier density of the normal state  $n$  approximately, and the calculated  $V_{coh} n_{pair}$  for different superconductors are also listed in Table II. Although the charge carrier density in unit coherent volume in FeSe is not very high, but it is still one order of magnitude larger than 1, and is much larger than that in Nb doped SrTiO<sub>3</sub> [67] which is supposed to be a system with dilute superfluid density. Therefore it is reasonable to argue that the Cooper pairs in the coherence volume  $V_{coh}$  in FeSe is diluted, and the superconducting transition should be close to the BCS-BEC crossover region. Our estimation on the Cooper pairs in one coherent volume tells that FeSe is not very different from other iron based superconductors, like BaK122, and is even close to some cuprate superconductors, like YBCO. This is consistent with the specific heat measurement [68] in Ba122, which shows a clear BCS mean-field like transition. It should be noted that SCF region in BaK122 is indeed very narrow as revealed by many different experimental tools.

Here we have observed a rather narrow region of SCF in FeSe above  $T_c$ , which is different from previous reports [29, 30]. One main difference is in the  $M$ - $T$  data, the authors there observed a very weak diamagnetic sig-



nal within a wide temperature range above the bulk  $T_c$  from the magnetization curves under high magnetic fields, which seems absent in our data. There are low-temperature upturn behaviors in our  $M$ - $T$  data instead of the constant positive background in previous report [30]. The measured upturn behaviors, which can be well described by the Curie-Weiss law, are mainly coming from the paramagnetic impurities such as interstitial iron impurities. One possible reason for the absence of strong SCF in our samples is that these paramagnetic impurities may suppress the SCF. These paramagnetic impurities may induce pair breaking to the preformed Cooper pairs above  $T_c$ , leading to a suppression on SCF. However, because the effective range of such a single impurity is very short, which is within about 10 Å in diameter as measured in Fe(SeTe) [69], and the distance between these interstitial Fe impurities is quite large, we think that such paramagnetic impurities are unlikely to behave as pair breakers to suppress the strong SCF. The relatively large  $RRR$  value also supports that the scattering from the diluted impurities is very weak. Furthermore, the very small residual specific heat coefficient measured in superconducting state indicates that the pair breaking by impurities is very weak [19]. One may argue that the SCF signal is buried in the upturn behavior of magnetic susceptibility from the paramagnetic impurities above  $T_c$ . We all know that the paramagnetic impurities are inevitable in a sample, however it should be noted that the upturn of magnetic susceptibility in our sample is very weak and can be well described by the Curie-Weiss law. This suggests that the SCF, if exists, would contribute really a negligible signal above  $T_c$ . Clearly, more data from samples of different groups are required to verify the SCF from magnetization measurements. However, based on our specific heat and Nernst data and thoughtful analysis mentioned above, we conclude that the SCF region in FeSe above  $T_c$  is rather narrow. Hence the superconducting transition is still governed by a BCS mean-field like critical transition. This indicates that even for a superconducting system with diluted Cooper pairs in the coherence volume, the SCF is still very limited and the

superconducting transition is still governed by the BCS mean-field like transition. This will stimulate to have a collective understanding on the critical behaviors for superconducting systems in the vicinity of BCS to BEC crossover.

## V. CONCLUSION

In conclusion, the superconducting fluctuation above  $T_c$  in FeSe seems very weak and the SCF region is very narrow from our experimental investigation using multiple tools, including magnetization, specific heat and Nernst. An revised calculation of the Ginzburg number  $Gi$  based on the standard method shows that it is rather small in bulk FeSe, and close to other iron based superconductors, such as BaK122. This explains our observation of a very narrow SCF region in bulk FeSe. A counting on the number of Cooper pairs in bulk FeSe finds that it is only about 31 in the coherent volume, which is two or three orders of magnitude lower than that of a typical conventional superconductor, suggesting that the system may be in the vicinity of the crossover between BCS and BEC. Theoretically it is highly desired to understand why the BCS mean-field like critical transition still holds for superconducting systems with such a diluted density of Cooper pairs.

## ACKNOWLEDGMENTS

We thank Yuji Matsuda, Christofer Meigast, and Tetsuo Hanaguri for helpful discussions. This work was supported by the National Key Research and Development Program of China (2016YFA0300401 and 2016YFA0401700), and National Natural Science Foundation of China (11534005).

\* huanyang@nju.edu.cn

† hhwen@nju.edu.cn

- 
- [1] I. I. Mazin, Nature (London) **464**, 183 (2010).
  - [2] K. Kuroki, S. Onari, R. Arita, H. Usui, Y. Tanaka, H. Kontani, and H. Aoki, Phys. Rev. Lett. **101**, 087004 (2008).
  - [3] G. R. Stewart, Rev. Mod. Phys. **83**, 1589 (2011).
  - [4] H. H. Wen and S. L. Li, Annu. Rev. Condens. Matter Phys. **2**, 121 (2011).
  - [5] F. C. Hsu, J. Y. Luo, K. W. Yeh, T. K. Chen, T. W. Huang, P. M. Wu, Y. C. Lee, Y. L. Huang, Y. Y. Chu, D. C. Yan, and M. K. Wu, Proc. Natl. Acad. Sci. USA **105**, 14262 (2008).
  - [6] C. L. Song, Y. L. Wang, P. Cheng, Y. P. Jiang, W. Li, T. Zhang, Z. Li, K. He, L. L. Wang, J. F. Jia, H. H. Hung, C. J. Wu, X. C. Ma, X. Chen, and Q. K. Xue, Science **332**, 1410 (2011).
  - [7] T. Shimojima, Y. Suzuki, T. Sonobe, A. Nakamura, M. Sakano, J. Omachi, K. Yoshioka, M. Kuwata-Gonokami, K. Ono, H. Kumigashira, A. E. Böhrer, F. Hardy, T. Wolf, C. Meingast, H. v. Löhneysen, H. Ikeda, and K. Ishizaka, Phys. Rev. B **90**, 121111 (R) (2014).
  - [8] K. Nakayama, Y. Miyata, G. N. Phan, T. Sato, Y. Tanabe, T. Urata, K. Tanigaki, and T. Takahashi, Phys. Rev. Lett. **113**, 237001 (2014).
  - [9] P. Zhang, T. Qian, P. Richard, X. P. Wang, H. Miao, B. Q. Lv, B. B. Fu, T. Wolf, C. Meingast, X. X. Wu, Z. Q. Wang, J. P. Hu, and H. Ding, Phys. Rev. B **91**, 214503 (2015).
  - [10] M. D. Watson, T. K. Kim, A. A. Haghighirad, N. R. Davies, A. McCollam, A. Narayanan, S. F. Blake, Y. L. Chen, S. Ghannadzadeh, A. J. Schofield, M. Hoesch, C.

- Meingast, T. Wolf, and A. I. Coldea, *Phys. Rev. B* **91**, 155106 (2015).
- [11] T. Terashima, N. Kikugawa, A. Kiswandhi, E. S. Choi, J. S. Brooks, S. Kasahara, T. Watashige, H. Ikeda, T. Shibauchi, Y. Matsuda, T. Wolf, A. E. Böhrer, F. Hardy, C. Meingast, H. v. Löhneysen, M. T. Suzuki, R. Arita, and S. Uji, *Phys. Rev. B* **90**, 144517 (2014).
- [12] M. D. Watson, T. Yamashita, S. Kasahara, W. Knafo, M. Nardone, J. Beard, F. Hardy, A. McCollam, A. Narayanan, S. F. Blake, T. Wolf, A. A. Haghighirad, C. Meingast, A. J. Schofield, H. v. Löhneysen, Y. Matsuda, A. I. Coldea, and T. Shibauchi, *Phys. Rev. Lett.* **115**, 027006 (2015).
- [13] J. P. Sun, K. Matsuura, G. Z. Ye, Y. Mizukami, M. Shimozaawa, K. Matsubayashi, M. Yamashita, T. Watashige, S. Kasahara, Y. Matsuda, J. Q. Yan, B. C. Sales, Y. Uwatoko, J. G. Cheng, and T. Shibauchi, *Nat. Commun.* **7**, 12146 (2016).
- [14] U. S. Kaluarachchi, V. Taufour, A. E. Böhrer, M. A. Tanatar, S. L. Budko, V. G. Kogan, R. Prozorov, and P. C. Canfield, *Phys. Rev. B* **93**, 064503 (2016).
- [15] P. S. Wang, S. S. Sun, Y. Cui, W. H. Song, T. R. Li, R. Yu, H. C. Lei, and W. Q. Yu, *Phys. Rev. Lett.* **117**, 237001 (2016).
- [16] T. Watashige, Y. Tsutsumi, T. Hanaguri, Y. Kohsaka, S. Kasahara, A. Furusaki, M. Sigrist, C. Meingast, T. Wolf, H. v. Löhneysen, T. Shibauchi, and Y. Matsuda, *Phys. Rev. X* **5**, 031022 (2015).
- [17] P. Bourgeois-Hope, S. Chi, D. A. Bonn, R. Liang, W. N. Hardy, T. Wolf, C. Meingast, N. Doiron-Leyraud, and L. Taillefer, *Phys. Rev. Lett.* **117**, 097003 (2016).
- [18] L. Jiao, C. L. Huang, S. Rößler, C. Koz, U. K. Rößler, U. Schwarz, and S. Wirth, *Sci. Rep.* **7**, 44024 (2017).
- [19] G. Y. Chen, X. Y. Zhu, H. Yang, and H. H. Wen, *arXiv:1703.08680v1* (2017).
- [20] P. O. Sprau, A. Kostin, A. Kreisel, A. E. Böhrer, V. Taufour, P. C. Canfield, S. Mukherjee, P. J. Hirschfeld, B. M. Andersen, and J. C. S. Davis, *arXiv:1611.02134v1* (2016).
- [21] Y. Wang, L. Li, and N. P. Ong, *Phys. Rev. B* **73**, 024510 (2006).
- [22] Z. W. Zhu, Z. A. Xu, X. Lin, G. H. Cao, C. M. Feng, G. F. Chen, Z. Li, J. L. Luo, and N. L. Wang, *New J. Phys.* **10**, 063021 (2008).
- [23] G. Sheet, M. Mehta, D. A. Dikin, S. Lee, C. W. Bark, J. Jiang, J. D. Weiss, E. E. Hellstrom, M. S. Rzchowski, C. B. Eom, and V. Chandrasekhar, *Phys. Rev. Lett.* **105**, 167003 (2010).
- [24] A. Pourret, L. Malone, A. B. Antunes, C. S. Yadav, P. L. Paulose, B. Fauqué, and K. Behnia, *Phys. Rev. B* **83**, 020504 (R) (2011).
- [25] A. Ramos-Álvarez, J. Mosqueira, F. Vidal, D. Hu, G. F. Chen, H. Q. Luo, and S. L. Li, *Phys. Rev. B* **92**, 094508 (2015).
- [26] F. Rullier-Albenque, D. Colson, A. Forget, and H. Alloul, *Phys. Rev. Lett.* **109**, 187005 (2012).
- [27] I. Pallecchi, F. Caglieris, and M. Putti, *Supercond. Sci. Technol.* **29**, 073002 (2016).
- [28] H. Yang, J. Xing, Z. Y. Du, X. Yang, H. Lin, D. L. Fang, X. Y. Zhu, and H. H. Wen, *Phys. Rev. B* **93**, 224516 (2016).
- [29] S. Kasahara, T. Watashige, T. Hanaguri, Y. Kohsaka, T. Yamashita, Y. Shimoyama, T. Mizukamia, R. Endo, H. Ikeda, K. Aoyama, T. Terashima, S. Ujie, T. Wolff, H. von Löhneysen, T. Shibauchi, and Y. Matsuda, *Proc. Natl. Acad. Sci. USA* **111**, 16309 (2014).
- [30] S. Kasahara, T. Yamashita, A. Shi, R. Kobayashi, Y. Shimoyama, T. Watashige, K. Ishida, T. Terashima, T. Wolf, F. Hardy, C. Meingast, H. v. Löhneysen, A. Levchenko, T. Shibauchi, and Y. Matsuda, *Nat. Commun.* **7**, 12843 (2016).
- [31] A. E. Böhrer, F. Hardy, F. Eilers, D. Ernst, P. Adelman, P. Schweiss, T. Wolf, and C. Meingast, *Phys. Rev. B* **87**, 180505 (R) (2013).
- [32] R. Werthamer, E. Helfand, and P. C. Hohenberg, *Phys. Rev.* **147**, 295 (1966).
- [33] Z. Tešanović, L. Xing, L. Bulaevskii, Q. Li, and M. Suenaga, *Phys. Rev. Lett.* **69**, 3563 (1992).
- [34] H. Gao, C. Ren, L. Shan, Y. Wang, Y. Z. Zhang, S. P. Zhao, X. Yao, and H. H. Wen, *Phys. Rev. B* **74**, 020505 (R) (2006).
- [35] H. H. Wen, W. L. Yang, Z. X. Zhao, and Y. M. Ni, *Phys. Rev. Lett.* **82**, 410 (1999).
- [36] J. Y. Lin, Y. S. Hsieh, D. A. Chareev, A. N. Vasiliev, Y. Parsons, and H. D. Yang, *Phys. Rev. B* **84**, 220507 (R) (2011).
- [37] V. J. Emery, and S. A. Kivelson, *Nature (London)* **374**, 434 (1995).
- [38] H. H. Wen, G. Mu, H. Q. Luo, H. Yang, L. Shan, C. Ren, P. Cheng, J. Yan, and L. Fang, *Phys. Rev. Lett.* **103**, 067002 (2009).
- [39] A. Junod, A. Erb, and C. Renner, *Physica C* **317-318**, 333 (1999).
- [40] K. Maki, *Physica* **55**, 124 (1971).
- [41] K. Behnia, and H. Aubin, *Rep. Prog. Phys.* **79**, 046502 (2016).
- [42] R. Bel, K. Behnia, and H. Berger, *Phys. Rev. Lett.* **91**, 066602 (2003).
- [43] Q. Tao, Z. W. Zhu, X. Lin, G. H. Cao, Z. A. Xu, G. F. Chen, J. L. Luo, and N. L. Wang, *J. Phys.: Condens. Matter* **22**, 072201 (2010).
- [44] M. Matusiak, Z. Bukowski, and J. Karpinski, *Phys. Rev. B* **81**, 020510 (R) (2010).
- [45] M. Matusiak, Z. Bukowski, and J. Karpinski, *Phys. Rev. B* **83**, 224505 (2011).
- [46] P. C. Li and R. L. Greene, *Phys. Rev. B* **76**, 174512 (2007).
- [47] G. Blatter, M. V. Feigel'man, V. B. Geshkenbein, A. I. Larkin, and V. M. Vinokur, *Rev. Mod. Phys.* **66**, 1125 (1994).
- [48] C. J. Lobb, *Phys. Rev. B* **36**, 3930 (1987).
- [49] Qiang Li, K. Shibusaki, M. Suenaga, I. Shigaki, and R. Ogawa, *Phys. Rev. B* **48**, 9877 (1993).
- [50] G. P. Malik, *J. Supercond. Nov. Magn.* **29**, 2755 (2016).
- [51] I. Pallecchi, M. Tropeano, G. Lamura, M. Pani, M. Palombo, A. Palenzona, and M. Putti, *Physica C* **482**, 68 (2012).
- [52] T. P. Orlando, K. A. Delin, S. Foner, E. J. McNiff, Jr., J. M. Tarascon, L. H. Greene, W. R. McKinnon, and G. W. Hull, *Phys. Rev. B* **36**, 2394 (R) (1987).
- [53] P. P. Nguyen, Z. H. Wang, A. M. Rao, M. S. Dresselhaus, J. S. Moodera, G. Dresselhaus, H. B. Radousky, R. S. Glass, and J. Z. Liu, *Phys. Rev. B* **48**, 1148 (1993).
- [54] P. Zimmermann, H. Keller, S. L. Lee, I. M. Savic, M. Warden, D. Zech, R. Cubitt, E. M. Forgan, E. Kaldis, J. Karpinski, and C. Krüger, *Phys. Rev. B* **52**, 541 (1995).

- [55] C. Buzea, and T. Yamashita, *Supercond. Sci. Technol.* **14**, R115 (2001).
- [56] A. D. Caplin, Y. Bugoslavsky, L. F. Cohen, L. Cowey, J. Driscoll, J. Moore, and G. K. Perkins, *Supercond. Sci. Technol.* **16**, 176 (2002).
- [57] H. Yang, H. Luo, Z. Wang, and H. H. Wen, *Appl. Phys. Lett.*, **93**, 142506 (2008).
- [58] C. Ren, Z. S. Wang, H. Q. Luo, H. Yang, L. Shan, and H. H. Wen, *Physica C* **469**, 599 (2009).
- [59] C. Tarantini, A. Gurevich, J. Jaroszynski, F. Balakirev, E. Bellingeri, I. Pallecchi, C. Ferdeghini, B. Shen, H. H. Wen, and D. C. Larbalestier, *Phys. Rev. B* **84**, 184522 (2011).
- [60] H. Ding, K. Nakayama, P. Richard, S. Souma, T. Sato, T. Takahashi, M. Neupane, Y. M. Xu, Z. H. Pan, A. V. Federov, Z. Wang, X. Dai, Z. Fang, G. F. Chen, J. L. Luo, and N. L. Wang, *J. Phys.: Condens. Matter*, **23**, 135701 (2008).
- [61] T. Terashima, N. Kikugawa, A. Kiswandhi, E. S. Choi, J. S. Brooks, S. Kasahara, T. Watashige, H. Ikeda, T. Shibauchi, Y. Matsuda, T. Wolf, A. E. Böhrer, F. Hardy, C. Meingast, H. v. Löhneysen, M. T. Suzuki, R. Arita, and S. Uji, *Phys. Rev. B* **90**, 144517 (2014).
- [62] M. Abdel-Hafiez, J. Ge, A. N. Vasiliev, D. A. Chareev, J. Van de Vondel, V. V. Moshchalkov, and A. V. Silhanek, *Phys. Rev. B* **88**, 174512 (2013).
- [63] A. Larkin and A. Varlamov, *arXiv:cond-mat/0109177v1* (2001).
- [64] F. Pistolesi and G. C. Strinati, *Phys. Rev. B* **49**, 6356 (1994).
- [65] D. van der Marel, J. L. M. van Mechelen, and I. I. Mazin, *Phys. Rev. B* **84**, 205111 (2011).
- [66] Y. J. Uemura, *Physica C* **282-287**, 194 (1997).
- [67] X. Lin, Z. W. Zhu, B. Fauqué, and K. Behnia, *Phys. Rev. X* **3**, 021002 (2013).
- [68] J. G. Storey, J. W. Loram, J. R. Cooper, Z. Bukowski, and J. Karpinski, *Phys. Rev. B* **88**, 144502 (2013).
- [69] J. X. Yin, Z. Wu, J. H. Wang, Z. Y. Ye, J. Gong, X. Y. Hou, L. Shan, A. Li, X. J. Liang, X. X. Wu, J. Li, C. S. Ting, Z. Q. Wang, J. P. Hu, P. H. Hor, H. Ding, and S. H. Pan, *Nat. Phys.* **11**, 543 (2015).